ORIGINAL ARTICLE

Numerical modeling of cohesive sediment transport in a tidal bay with current velocity assimilation

Peng Zhang · Onyx W. H. Wai · Jianzhong Lu · Xiaoling Chen

Abstract Tidal currents play an important role in sediment dynamics in coastal and estuarine regions. The goal of this study is to investigate the effects of current velocity assimilation (CVA) on sediment transport modeling in tide-dominated waters. A hydrodynamic and sediment transport model for Deep Bay, Hong Kong, was established based on a three-dimensional primitive equation Finite Volume Coastal Ocean Model. An additional numerical simulation was conducted with in situ current velocity measurements sequentially assimilated into the model using a three-dimensional optimal interpolation scheme. The performance of CVA shows improvements in the root-mean-square errors and average cosine correlations of simulated current velocity by at least 9.1 % and 10.3 %, respectively. Moreover, the root-mean-square error of the simulated sediment concentration from the model with CVA was decreased by at least 7 %. A reasonable enhancement in the vertical and spatial distributions of sediment concentrations was demonstrated from the simulation results from the model with CVA. It was found that the bottom shear stress changed significantly when the simulated velocities were corrected with CVA. The results suggest that CVA has the potential to improve sediment transport prediction because tidal currents dominate sediment dynamics in the studied areas.

Keywords Numerical model · Sediment transport · Current velocity assimilation · FVCOM · Deep bay

1 Introduction

Powerful numerical models for predicting the transport and fate of sediments in coastal waters are essential for a variety of environmental problems related to coastal engineering, pollution nutrient transport and wetland preservation (Warner et al. 2008). Investigations of the complicated sediment dynamics using numerical models are urgent for Deep Bay, a shallow embayment located between Hong Kong and the Chinese mainland. Many environmental problems have been generated in the bay, including high turbidity of the affected waters by major construction and land reclamation projects and significant wetland contamination by heavy metals and nutrient sediment pollution. However, reports on developing numerical models to help understand hydrodynamic and sediment transport in Deep Bay are rare.

Hydrodynamic action is the most important mechanism involved in sediment transport. It provides the forces for horizontal advection and bed erosion and plays a major role in the flocculation of cohesive sediments (Cancino and Neves 1999). Deep Bay is an active tidal shelf environment with a tidal elevation range as large as 2.5 m and current velocities exceeding 1 m/s (Qian 2003). Sediment

P. Zhang
Key Laboratory of Ecological Impacts of Hydraulic-Projects and Restoration of Aquatic Ecosystem of Ministry of Water Resources, The Institute of Hydroecology, Ministry of Water Resource and Chinese Academy of Sciences, Wuhan 430079, China
e-mail: peterwin86@gmail.com

P. Zhang · J. Lu (✉) · X. Chen
State Key Laboratory of Information Engineering in Surveying, Mapping and Remote Sensing, Wuhan University, Wuhan 430079, China
e-mail: lujzhong@126.com

O. W. H. Wai
Department of Civil and Environmental Engineering, The Hong Kong Polytechnic University, Kowloon, Hong Kong, China

movement and bottom resuspension under normal conditions and without significant wind-induced waves appear to be primarily controlled by tidal currents (Grochowski et al. 1993; Guillou and Chapalain 2010). In such an environment, tidal waters periodically flow in and out of the bay, dominating sediment transport patterns. Sediments are eroded and transported upward during flood tide and deposited later onto the bottom during slack water periods. The sediments are then eroded again and transported downward during ebb tide and redeposited during the next slack water until the start of the next tidal cycle (Cancino and Neves 1999). Therefore, only accurate hydrodynamic simulations will provide sufficient sediment modeling results.

However, hydrodynamic models inevitably contain several sources of uncertainty that can reduce the forecast accuracy at every model stage. Certain errors may inherently exist in the governing equations that imperfectly describe the complex physical processes and their interactions. These errors are often related to the simplification of equations in numerical computation. Uncertainty can also occur due to an incorrect prescription of the model parameters and model input data, e.g., bathymetry and initial and boundary conditions. Data assimilation provides a useful tool to reduce these uncertainties and improve model results. By integrating model forecasts with measurement data based on uncertainty information in the model and measurements, data assimilation techniques can prevent the model from deviating too far from reality and thus achieve better model forecasts. Much work has been devoted to studying current velocity assimilation. The efficiency of current velocity assimilation has been demonstrated by experiments that directly assimilate current velocities measured with shipboard Acoustic Doppler Current Profilers (ADCP) (Kurapov et al. 2005; Zhang et al. 2007; Jordi and Wang 2013). In addition, assimilation of current velocities derived from high-frequency radars also exhibits a large potential for improving hydrodynamic forecasting in coastal waters (Paduan 2004; El Serafy and Mynett 2008; Barth et al. 2010). By using data assimilation, the covariance error statistic and the close relationships between different model variables guarantee that a single observation updates not only the corresponding state variable but also other unobserved state variables. Kurapov et al. assimilated velocity data obtained from a moored ship into a model of coastal wind-driven circulation off Oregon. The assimilated data had a positive effect on the predictions of sea surface height, temperature, potential density and surface salinity. Because data assimilation can affect the bottom boundary layer (BBL) by correcting velocities close to the bottom, they also noted a significant improvement in predicting turbulence dissipation rates and the BBL shear stress magnitudes, all of which are closely related to BBL sediment motion (Kurapov et al. 2005). However, Kurapov et al. did not directly show any related results and discussion about sediment prediction improvements by verifying with sediment measurements, and did not discuss to what extent the sediment prediction was affected by current velocity assimilation, especially in coastal waters and estuaries where sediment movement is dominated by tidal currents.

It is noted that there have been some studies on improving numerical modeling of sediment transport by data assimilation methods. These studies were dedicated to assimilating remote sensing sediment to investigate the positive effect on sediment transport modeling (EI Serafy et al. 2011; Margvelashvili et al. 2013; Zhang et al. 2014). However, as discussed above, hydrodynamics is the most important force of sediment transport. Ignoring achieving effective hydrodynamic numerical simulation would not help to fundamentally improve the accuracy of sediment transport modeling. Considering the above points, the goal of this research was to explore the effect of current velocity assimilation on sediment transport modeling, taking a tide-dominated bay, Deep Bay in Hong Kong, as a study case.

The rest of this paper is organized as follows. Section 2 describes the hydrodynamic and sediment transport model and the model established for Deep Bay. The current velocity assimilation (CVA) method is also briefly presented in this section. In Sect. 3, the CVA results and CVA effects on sediment transport are discussed after presenting the model calibration and validation results. Conclusions are drawn and given in the last section.

2 Methodology

2.1 Study domain and in situ measurements

Deep Bay (22.41–22.53°N,113.88–114.00°E) is a semi-enclosed, shallow bay on the eastern side of the Pearl Estuary between Shenzhen to the north and the New Territories of Hong Kong to the south (Fig. 1). The average water depth of the bay is about 2.9 m and the maximum water depth is less than 5.0 m. The width of the bay is from 4 to 7.6 km at the narrowest section near the mouth. The length is 13.9 km and the total sea surface area is about 80 km². Four rivers flow into the bay (Fig. 1). Because of its unique geographic location and coastline geometry, the embayment exhibits its own water environment. Hydrographic survey data displayed by Wong and Li (1990) showed that the depth-averaged current speed ranged from 0.11 to 0.32 m/s. The salinity varied from 4 to 22 ppt in the wet season due to the strong water stratification. In the dry season, the water was well mixed and the salinity ranged from 26 to 32 ppt. The average suspended solids
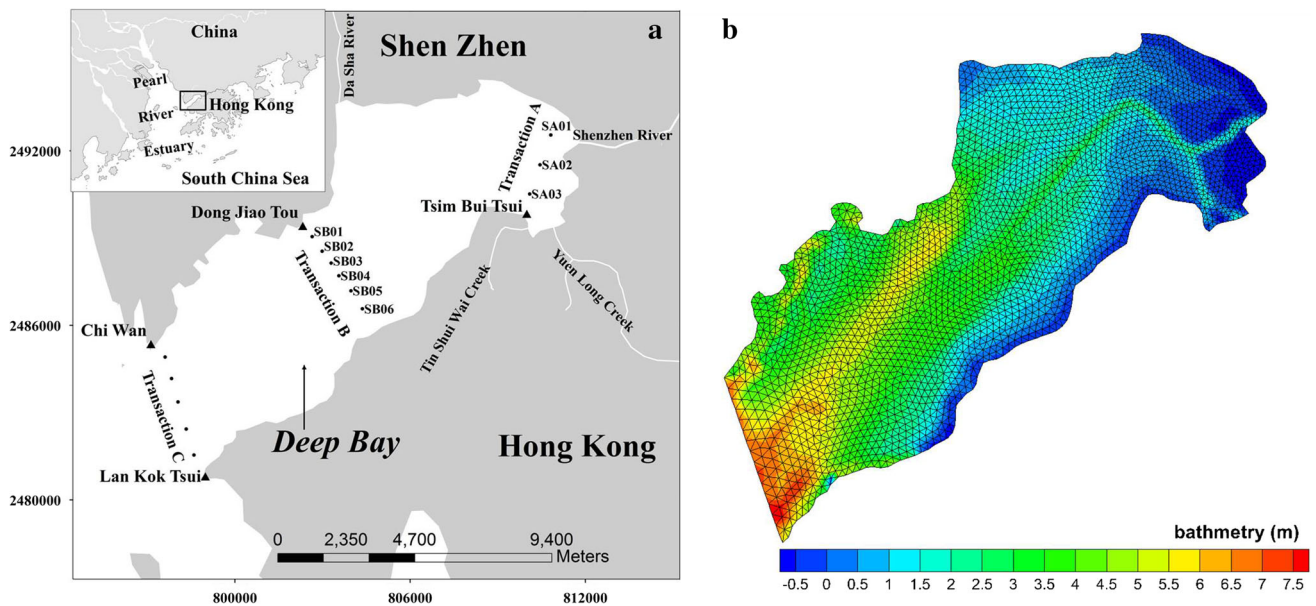
Fig. 1 Study area location (*left, upper corner*) and measurement sites (*filled triangle* water level stations and *filled circle* sites that measured the current velocity and sediment concentration), and model grids and bathymetry (*right*). Note that the study area map is projected onto the Cartesian coordinate system using the UTM projection

concentrations in the dry season and the wet season were about 50 and 10 mg/L, respectively. The particle size of suspended sediment in Deep Bay has a marked seasonal variation. The median size of suspended sediment in the dry season and the wet season were about 10 and 2.7 μm, respectively.

Measurements used in this study are parts of the synchronous survey project commenced in June 2005 in Shenzhen River basin, which were conducted by the Hydrology Bureau of the Yangtze River Water Resources Commission of China. Measurements used in this study were recorded hourly over two phases at each site shown in Fig. 1. The first phase occurred during a neap tide between 10:00 am on June 16 and 17:00 pm on June 17 (a total of 30 h). The second phase occurred during a spring tide between 08:00 am on June 23 and 12:00 pm on June 24 (a total of 29 h). Water levels were taken hourly by means of tidal gauges placed at Dong Jiao Tou (DJT), Tsim Bui Tsui (TBT), Chi Wan and Lan Kok Tsui (see Fig. 1). Vertical profiles of flow velocity, sediment concentration, and salinity were collected hourly at sites located along three Transections inside the bay. Transection A is to the northeast of Deep Bay near the mouth of the Shenzhen River. There are three observation sites: SA01, SA012 and SA03. Transection B is in the middle of the bay and includes six observation sites: SB01, SB02, SB03, SB04, SB05 and SB06. Transection C is at the mouth of Deep Bay, almost parallel to Transection B and includes five observation sites. The measured data in Transection C were not used for calibration or validation purposes, but as

boundary condition data. According to the water depth h (m) at local measurement time, the velocity measurements were obtained at six vertical levels: $0.0h$ (surface layer), $0.2h$ (near-surface layer), $0.4h$, $0.6h$, $0.8h$ (near-bottom layer) and $1.0h$ (bottom layer). At each site, current velocities were measured hourly by the ZSX-3 direct-reading flow instrument at each vertical layer. Water samples were collected sequentially from the surface layer to the bottom layer at each site. Five hundred milliliters of each water sample was taken and filtered immediately on a pre-weighted Whatman Cellulose Acetate Membranes filter with a diameter of 47 mm and a nominal pore size of 0.45 μm. The filter was stored in a desiccator, which was then combusted in a 500 °C oven for 3 h and weighed in the laboratory. An analytical balance was used to weigh the filter, with a precision of 0.01 mg. Sediment concentration was determined by the weight difference normalized by the filtered water volume. Salinities were measured by a digital salinity meter from these water samples and temperature was recorded by water thermometers. It should be noted that when water depth was less than 2 m, measurements were not taken at surface layer ($0.0h$) and bottom layer ($1.0h$), especially at the sites in Transection A because of very low water depths at most of the time in a tidal cycle.

2.2 Numerical model description and configuration

The model used to calculate the hydrodynamics of Deep Bay was an unstructured-grid, Finite Volume, free-surface, 3-D primitive equation, Finite Volume Coastal Ocean

Model (FVCOM) developed by Chen et al. (2003, 2006). Unstructured triangular grids used in FVCOM provide an accurate fit for the geometry of irregular coastlines. A sigma-coordinate transformation was used to represent bottom slope irregularities in the vertical direction. The model simulates water surface elevation, 3D velocity, flooding and drying processes, temperature, salinity, water quality and sediment transport. A full description of the hydrodynamic continuity equation and the numerically discrete FVCOM scheme is given by (Chen et al. 2003).

The sediment transport model in FVCOM is based on the Community Sediment Transport Model (CSTM) developed in collaboration with the US Geological Survey (USGS). which includes suspended sediment and bedload transport, layered bed dynamics based on active layer concept, flux-limited solution of sediment setting, unlimited number of sediment classes and bed layers, and cohesive sediment erosion/deposition algorithms. The model has been tested in many coastal environment studies for the calculation of current-induced erosion, transport, and the deposition of cohesive sediment (Lettmann et al. 2010; Wu et al. 2011).

Through analyzing size distribution of suspended sediment from field survey data of Deep Bay by Wong and Li (1990), it was argued that the median size of suspended sediment in the wet season is 2.7 μm and there is no significant difference in the size distribution of suspended sediment in the vertical direction. In this study, only cohesive sediment with a dominant median size of the suspended matter was considered to simulate three-dimensional sediment transport of Deep Bay by FVCOM.

The sediment transport model in FVCOM solves the three-dimensional advection–dispersion equation.

$$\frac{\partial C}{\partial t} + \frac{\partial uC}{\partial x} + \frac{\partial vC}{\partial y} + \frac{\partial(w - W_s)C}{\partial z} = \frac{\partial}{\partial x}\left(A_H\frac{\partial C}{\partial x}\right) + \frac{\partial}{\partial y}\left(A_H\frac{\partial C}{\partial y}\right) + \frac{\partial}{\partial z}\left(K_H\frac{\partial C}{\partial z}\right) \quad (1)$$

where C is the sediment concentration, W_s is the settling velocity, u, v, and w are the three components of the velocity vector, and A_H and K_H is the horizontal and vertical eddy diffusivity coefficients, respectively. In the model, the modified Mellor and Yamada level-2.5 (MY-2.5) turbulence closure model (Mellor and Yamada 1982; Galperin et al. 1988) is used for the parameterization of vertical eddy diffusivity coefficient. The Smagorinsky formula is used for calculation of the horizontal diffusivity coefficients (Smagorinsky 1963).

At the surface, a no-flux boundary condition is used for the sediment concentration:

$$K_H\frac{\partial C}{\partial z} - W_sC = 0, \quad z = \xi \quad (2)$$

At the bottom, the sediment flux is the difference between deposition and erosion.

Table 1 Calibrated parameters in the Deep Bay model

Parameters	Symbol	Value
Bottom roughness coefficient in Eq. (8)	z_0	0.0024 m
Critical shear stress for deposition in Eq. (5)	τ_{cd}	0.08 N m^{-2}
Critical shear stress for erosion in Eq. (6)	τ_{ce}	0.2 N m^{-2}
Erosion constant in Eq. (6)	E_b	1.2×10^{-5} kg m^{-2} s^{-1}
Constant value of settling velocity in Eq. (9)	W_0	8.5×10^{-5} m/s
Critical sediment concentration in Eq. (9)	C_0	50 mg/L
Empirical coefficients in Eq. (9)	k,m	0.014, 1.5

$$K_H\frac{\partial C}{\partial z} - W_sC = R_D - R_E, \quad z = -H \quad (3)$$

where R_D is the deposition rate, R_E is the bed erosion rate, ξ is water surface elevation above a specified datum, and H is bathymetric depth below the datum.

In the model, the above equations are transformed into the σ-coordinate in the vertical in order to obtain a smooth representation of irregular bottom topography, and then resolved by the finite volume method. The σ-coordinate transformation is defined as

$$\sigma = \frac{z - \xi}{H + \xi} = \frac{z - \xi}{D} \quad (4)$$

where σ varies from -1 at the bottom to 0 at the surface, and D is water depth.

In this work, the cohesive sediment deposition rate is calculated using Krone's worldwide deposition formula (Krone 1962). The bed erosion rate of cohesive sediment is determined by the classic formula given by Partheniades (1965). The formulas are

$$R_D = \begin{cases} W_sC_b\left(1 - \tau_b/\tau_{cd}\right) & \text{for} \quad \tau_b < \tau_{cd}, \\ 0 & \text{for} \quad \tau_b \geq \tau_{cd} \end{cases} \quad (5)$$

$$R_E = \begin{cases} E_b\left(\tau_b/\tau_{ce} - 1\right) & \text{for} \quad \tau_b > \tau_{ce}, \\ 0 & \text{for} \quad \tau_b \leq \tau_{ce} \end{cases} \quad (6)$$

where C_b is the near-bottom layer concentration, E_b is the erosion constant, τ_{cd} is the critical shear stress of deposition, τ_{ce} is the critical shear stress of erosion, and τ_b is the bed shear stress. The x and y components of the bed shear stresses are

$$(\tau_{bx}, \tau_{by}) = C_d\sqrt{u_b^2 + v_b^2}(u_b, v_b) \quad (7)$$

where u_b and v_b are the x and y components of near-bottom velocity. The drag coefficient C_d is determined by

matching a logarithmic bottom layer to the model at a height z above the bottom and calculated as

$$C_{\mathrm{d}} = \max(k_v^2/\ln(z/z_0)^2, 0.0025) \tag{8}$$

where $k_v=0.4$ is the von Karman's constant and z_0 is the bottom roughness coefficient, which is need to be calibrated by field measurements (see Table 1).

The settling velocity W_s of cohesive sediment (in Eq. 9) is one of the most important vertical sediment motion parameters and is difficult to determine. In this study, a well-known power law was used to calculate the setting velocity. The power law that represents an exponential relationship between the settling velocity and sediment concentration (Eq. 9) was used to calculate the settling velocity when the sediment concentration is higher than a constant value. When the sediment concentration is less than the critical or constant sediment concentration, a free settling velocity is used (Lumborg and Windelin 2003; Krone 1962). The setting velocity is calculated as

$$W_s = \begin{cases} kC^m & \text{for } C \geq C_0 \\ W_0 & \text{for } C < C_0 \end{cases} \tag{9}$$

where C is sediment concentration, C_0 is the critical sediment concentration, W_0 is the constant value of settling velocity, and k and m are empirical coefficients that need to be calibrated by field measurements (see Table 1). This settling velocity equation is widely used in various estuarine and coastal models and in Hong Kong studies because it allows some flexibility in the settling velocity values for cohesive sediment particles.

The model grids used for the Deep Bay were generated under the Cartesian coordinate system based on the land boundary with a relatively high resolution (80 m) in the inner bay near the Shenzhen River and a coarser resolution (250 m) at the open boundary (see Fig. 1). Because the in situ measurement were conducted at 0.0h, 0.2h, 0.4h, 0.6h, 0.8h, 1.0h (h is water depth), Six vertical sigma layers were set in the model in order to facilitate model calibration and validation. The model run time extended from 00:00 am on June 10 to 24:00 pm on June 25 2005. The external and internal time steps were 1 and 10 s, respectively. Hourly wind metrological data at TBT obtained from the Hong Kong Observatory were used for the spatial-uniform water surface driving force. The open boundary was driven by tidal elevations measured at Chi Wan and Lan Kok Tsui. Measured sediment concentrations, salinity and temperature at Transection C sites were also prescribed in the open boundary. The freshwater flow rate and sediment concentration discharged into Deep Bay from the Shenzhen, Yuen Long, Tin Shui Wai and Da Sha Rivers were prescribed. The model was cold-started and initialized with zero current velocity. Because the

model initial time was in the neap tide period, the sediment concentrations, salinity and temperature were initialized using horizontally uniform values with the mean observed profiles measured from 10:00 am on June 16 to 15:00 pm on June 17. The tidal amplitude was initialized using in situ measured water levels at TBT obtained from the Hong Kong Observatory. The model was spun-up for more than a tidal cycle until 10:00 am on June 16 when the calibration experiment was conducted.

2.3 Current velocity assimilation scheme

2.3.1 Assimilation approach

In this study, the optimal interpolation algorithm was employed as the assimilation approach. This algorithm has been successfully applied to assimilate current velocity in improving current forecasts for its relatively low cost in computation in highly nonlinear and high-dimensional ocean models. Based on the optimal interpolation method, the updated current velocity field with assimilation is derived from the following equation:

$$V_k^a = V_k^f + W_k(V_k^o - V_k^f) \tag{10}$$

where V_k^a are the updated current velocities, V_k^f are the model forecasted current velocities, V_k^o are the in situ-measured current velocities, k indicates the assimilation time, and W_k is the weights matrix, which is obtained by minimizing the error covariance of the updated current velocity field V_k^a

$$W_k = P^f(P^f + R_k)^{-1} \tag{11}$$

Through Eq. (10), optimal interpolation arbitrarily locates observations by interpolation within a model grid using a model forecast field as a first guess. Therefore, the updated field is at an optimal state. The model is then integrated to the next forecast time with this field as the initial condition until the next assimilation time.

When carrying out optimal interpolation, it is often assumed that measurement noise follows a Gaussian distribution and is uncorrelated with model errors and that no correlation between measurement errors exists. In this study, considering that the measurement errors were relatively very small, it was assumed that the measurements were error-free in the assimilation procedure. Based on this assumption, different forecast error variances at each assimilation time can be obtained with the following formula:

$$\sigma_k^2 = \frac{1}{N}\sum_{j=1}^{N}(V_{k,j}^f - V_{k,j}^o)^2 \tag{12}$$

where σ_k^2 is forecast or background error variance at time k, $V_{k,j}^f$ and $V_{k,j}^o$ are the forecasted and measured current velocity at the jth location, and N indicates the number of measurements at time k. The covariance is typically defined as a function of a forecast error correlation model because it can be derived by multiplying the correlation by the variance. Many schemes for calculating forecast error correlations have been proposed and implemented in assimilation applications (Larsen et al. 2007; Høyer and She 2007). It is typically assumed that the horizontal and vertical forecast error correlations decrease exponentially with the square of the distance, which is specified as

$$\rho = \exp\left[-\frac{(\Delta x)^2 + (\Delta y)^2}{R_1^2} - \frac{(\Delta z)^2}{R_2^2}\right], \qquad (13)$$

where ρ is the forecast error correlation, $\Delta x, \Delta y,$ and Δz are the distances between two forecast points in the $x, y,$ and z directions, and R_1 and R_2 are the horizontal and vertical correlation lengths, respectively, which are used to limit the influence of a single observation in the interpolation procedure within a fixed region around the observation location (Xie and Zhu 2010). To ensure the effectiveness of current velocity assimilation, suitable correlation lengths in the horizontal and vertical direction need to be determined. In this study, the vertical correlation radius R_2 was specified as the maximum sigma depth (1.0) to ensure that the measurement in each layer is influenced in the column. For the estimation of the horizontal correlation radius R_1 in this study, a cross-validation method, similar to the approach adopted by Zhang et al. (2007) was used. By comparing the error statistics between the model and the CVA results, the optimal value of R_1 was selected. This value was expected to ensure that the CVA results would show the greatest current velocity improvements.

In this study, the assimilation experiment was implemented through an optimal interpolation FORTRAN module with the Octave interface in the Linux environment. The measured velocities at the six vertical levels from the three Transections were assimilated into the model in the experiment. To verify that the current velocity assimilation was valid, measurements at SA02 and SB03 were used to compare with the assimilation results. Therefore, data from these locations were not used in the assimilation process.

2.3.2 Analysis of the results

In this study, the assimilation effectiveness was quantified using the improvement in the root-mean-square error (RMSE), which was calculated as the relative decreases in RMSE (Eq. (14) below), and the improvement in the average cosine correlation (ACC), which was calculated as the relative increase in ACC (Eq. (15) below).

$$\text{RMSE improvement} = \frac{\text{RMSE}_1 - \text{RMSE}_2}{\text{RMSE}_1} \times 100\,\%, \qquad (14)$$

$$\text{ACC improvement} = \frac{\text{ACC}_2 - \text{ACC}_1}{\text{ACC}_1} \times 100\,\%, \qquad (15)$$

where RMSE_1 and RMSE_2 are RMSEs of the simulated velocity from the model without and the model with CVA and ACC_1 and ACC_2 are ACCs of the simulated velocity from the model without and the model with CVA. The RMSE for each site was calculated as

$$\text{RMSE} = \sqrt{\frac{\sum_{i=1}^n (V_i^{\text{model}} - V_i^{\text{insitu}})^2}{n}}, \qquad (16)$$

where V^{model} is the magnitude of the simulated velocity from the model without or the model with CVA, V_i^{insitu} is the magnitude of the in situ-measured current velocity, and n is the number corresponding to the assimilation time. The ACC for each site was computed as

$$\text{ACC} = \frac{1}{n}\sum_{i=1}^n \cos\theta_i = \frac{1}{n}\sum_{i=1}^n \frac{u_1 u_2 + v_1 v_2}{\sqrt{(u_1^2 + v_1^2)(u_2^2 + v_2^2)}}, \qquad (17)$$

where $\cos\theta_i$ is the cosine of the angle between the in situ-measured current velocity vector u_1, v_1 and the simulated velocity vector u_2, v_2 at time i. The formula denotes the correlation between two vectors. The resulting value of $\cos\theta_i$ ranges from -1 to 1 and indicates the correlation between two velocity vectors. The higher this value is, the greater the similarity.

3 Results and discussion

3.1 Model calibration and validation

3.1.1 Calibration results

The model reached an equilibrium state after several tidal cycles of the spin-up time. Model calibration was then carried out for the neap tide period (10:00 am on June 16 to 15:00 hpmours on June 17), when 30 h of measured data were collected. Model calibration was conducted using a simple trial-and-error method by manually refining the hydrodynamic and sediment transport parameters to match the model results with the measured data. Firstly, a selection of parameters with specified physical hydrodynamic model meanings, including river discharge, bathymetry and open boundary condition, and empirical parameters, including the bottom friction coefficient, were adjusted so that the simulated water levels and current velocities matched the measurements. The sediment transport model parameters were
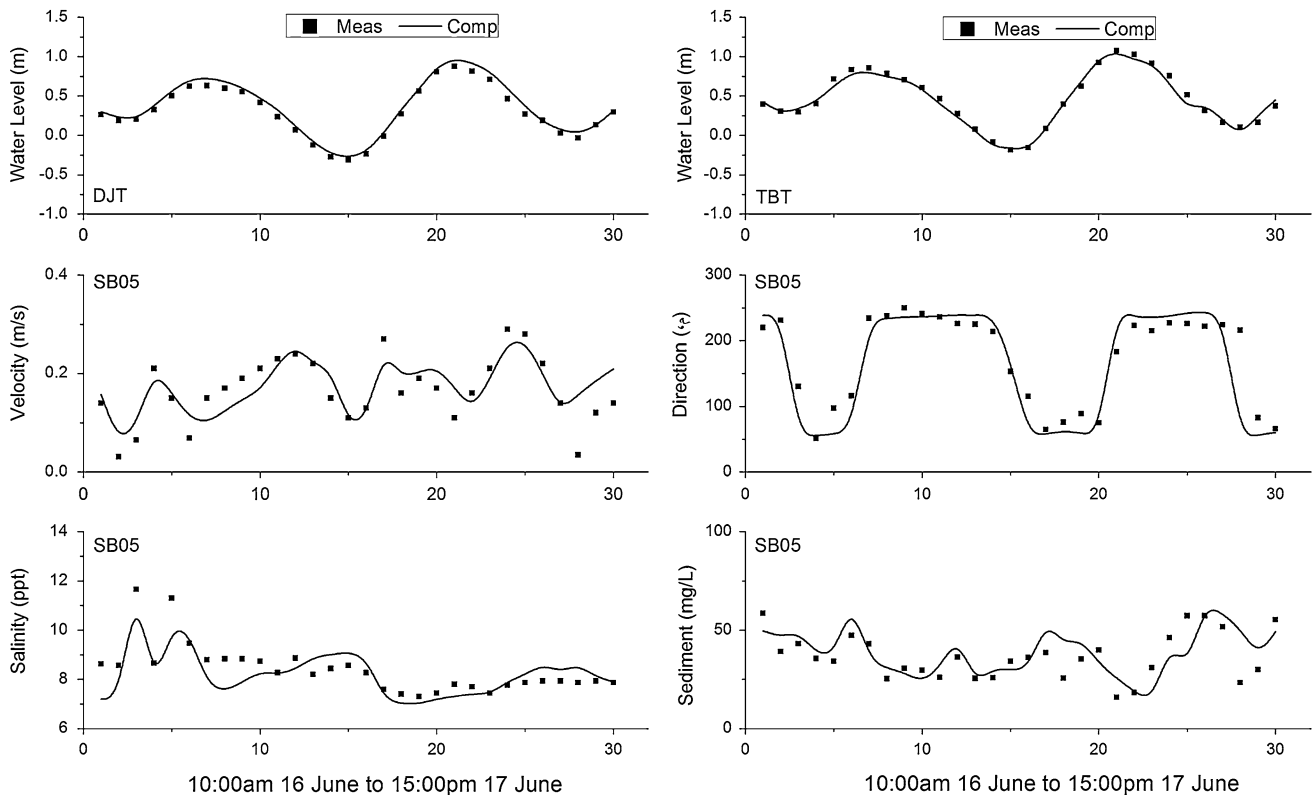
Fig. 2 Comparison of water levels, depth-averaged current velocity, current direction, salinity and sediment concentration with model results during the calibration period at SB05. *Meas* measurements and

Comp computed results from the reference model or the model without CVA (mentioned in the later sections)

adjusted by comparing the model results with the observed data at the measurement sites. After repeated adjustments, an optimal series of parameters was selected for the hydrodynamic and sediment transport modeling of Deep Bay. These final parameters are listed in Table 1. In Fig. 2, the time series of the water level at the two tidal stations and depth-averaged current velocity magnitude, current direction, salinity and sediment concentrations at site SB05 are compared with the model results for the calibration period. The comparison shows that the computed hydrodynamic and sediment transport results are consistent with the measurements. The RMSEs of simulated water level at the two tidal stations are less than 6.7 cm. For all sites during the calibration period, the ACCs of simulated current velocity are greater than 0.71 and the RMSEs of simulated current velocity, salinity and sediment concentration are less than 0.16 m/s, 0.65 ppt and 31.5 mg/L, respectively.

3.1.2 Model validation with measurements

After a satisfactory model calibration, the model was validated with measurements in the second phase (08:00 am on June 23 to 12:00 am on June 24), when there were 29 h of measurements. Figure 3 shows a comparison between

model results and measurements. The time series of the simulated tidal elevation at DJT and TBT and salinity at sites SA03 and SB05 show a satisfactory consistency with in situ measurements. The RMSEs of simulated tidal elevation at DJT and TBT are 7 and 11 cm, respectively. The RMSEs of simulated salinity for all the stations are less than 0.52 ppt. To help analyze the performance of the current circulation model, the time series of depth-averaged current velocity magnitude and direction from the model are verified with measurements at sites SA03 and SB05 (Fig. 3). Comparisons show that the simulated current velocity results correlate properly with the current velocity measurement during the flood and ebb tide phases. However, a better consistency between model results and measurement can be found at site SB05 than that at site SA03. Statistics displayed in Table 2 also show that most sites on Transection B have relatively smaller RMSEs and larger ACCs than sites on Transection A. The sediment transport modeling results are validated against the measured sediment concentrations at site SA03 and site SB05 at the near-surface and near-bottom layers (Fig. 3). Although erroneously deviated from measurements at some model times, the sediment model results are generally closed to the dynamic trend represented in the measurements.
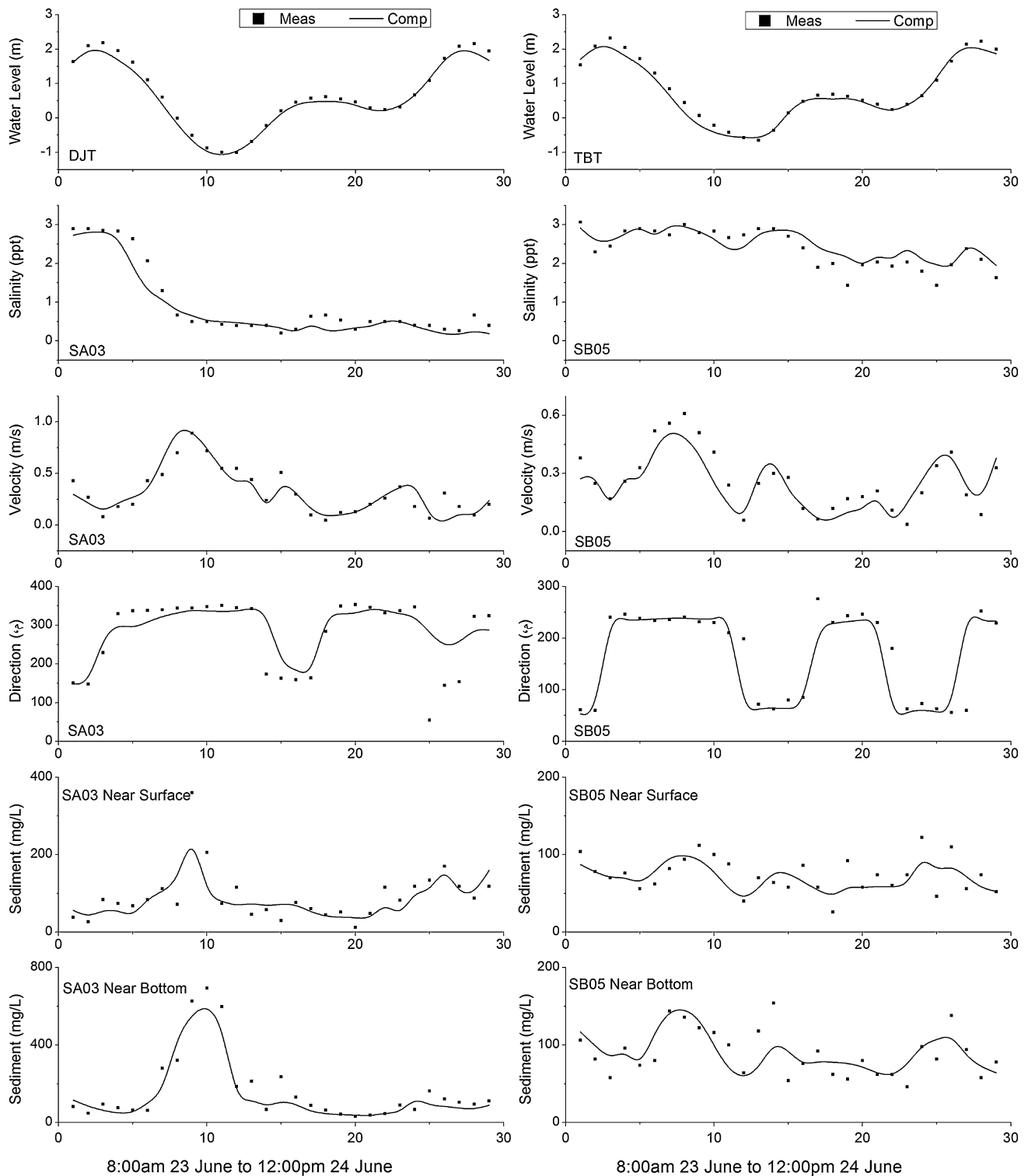
Fig. 3 Water level validation at two tidal stations and depth-averaged current velocity, current direction, salinity and sediment concentration validation at sites SA03 and SB05

A comparison of sediment concentration with current velocity magnitude in Fig. 3 shows that sediment concentrations at both the near-surface layer and near-bottom layer exhibit a dynamic trend that is similar to the complicated dynamic of current velocities at sites SA03 and SB05. This finding indicates that sediment transport is

closely related to the flow current dynamics of the bay. The RMSE statistics for the simulated sediment concentration displayed in Table 3 shows that the errors at all sites on Transection A are larger than those at sites on Transection B. This finding could be associated with more accurate modeling of current velocity in the middle of the bay, further revealing that in this tidally driven bay, the tidal current is of great importance to sediment dynamics. Therefore, only current velocity predicted with a high degree of model accuracy can produce reliable sediment dynamic modeling.

3.2 CVA results

Although the calibrated model produced a good hydrodynamic and sediment dynamic representation as a whole, the results did not always accurately reproduce the values of the variables at some sites. An additional model simulation was conducted in which hourly measured velocities at six vertical levels were assimilated into the model using optimal interpolations, as described above in Sect. 2.3.2. As noted in that section, the horizontal correlation radius must be determined using a readily available empirical method. A series of assimilations was repeatedly made by changing the horizontal correlation radius without assimilating measurements from the SA02 and SB03 sites. Trials with 1000, 1200, 1400,…, 6000 m were conducted. The RMSE and ACC were calculated for each correlation radius during the assimilation period. It was found that when the correlation radius reached 3800 m, the optimal RMSE and ACC improvement was achieved at the two sites. Table 2 shows the summary of the RMSE and ACC values and their improvement in relation to the two

validation sites when CVA simulations were made. It can be seen that the RMSE improvement is greater than 35 % and ACC improvement is greater than 14 %. A comparison between measured depth-averaged velocities and computed results from the model with and without CVA for sites SA02 and SB03 is shown in Fig. 4, demonstrating that the model with CVA produces results that better agree with the measurements and more reasonably reproduces the current velocity dynamics at the two verification sites.

Through data assimilation, observations are integrated into the model, subsequently updating the simulated velocities at the measurement locations. A statistical comparison between the depth-averaged current velocities at the assimilation sites is shown in Table 2. Clear improvements in ACC and RMSE values are found at all assimilation sites, particularly sites SA03 and SB04. For most sites, the RMSEs are improved by at least 23.5 % and the ACCs are improved by 10.3 %. The RMSE mostly decreased to less than 0.1 m/s while the ACC increased to greater than 0.9. Figure 5 shows the comparisons of vertical profiles of velocity from measurements and the simulated results from the model with and without CVA at 10:00 am on June 23. It can be seen from the comparisons that the CVA reproduced velocity profiles those better agree with the measurements both at the assimilation sites (SA03 and SB05) and the verification sites (SA02 and SB03). Therefore, the simulated depth averaged velocities were improved in the model with CVA.

The simulated current velocities close to the measurement sites were affected by spatially interpolating subsets of the nearby velocity measurements. Such cases were not only observed at sites SA02 and SB03 (no assimilation), as mentioned above. Figure 6 shows the simulated spatial

Table 2 Comparison of RMSE (m/s) and average cosine correlation (ACC) of depth-averaged current velocity between models with and without CVA at the assimilation and verifying sites

| Sites	Model without CVA		Model with CVA		Improvement (%)	
	RMSE	ACC	RMSE	ACC	RMSE	ACC
Validation sites						
SA02	0.17	0.61	0.11	0.72	35.3	18.0
SB03	0.13	0.83	0.05	0.95	61.5	14.5
Assimilation sites						
SA01	0.17	0.69	0.13	0.78	23.5	13.0
SA03	0.1	0.7	0.06	0.83	40.0	18.6
SB01	0.09	0.85	0.06	0.95	33.3	11.8
SB02	0.11	0.82	0.1	0.91	9.1	11.0
SB04	0.14	0.87	0.08	0.96	42.9	10.3
SB05	0.07	0.86	0.05	0.95	28.6	10.5
SB06	0.12	0.79	0.08	0.88	33.3	11.4

Table 3 RMSE (mg/L) of sediment concentration between models with and without CVA

Sites	Model without CVA		Model with CVA		RMSE improvement[a](%)	
	Near-surface	Near-bottom	Near-surface	Near-bottom	Near-surface	Near-bottom
SA01	8.5	39.2	7.2	19.7	15.3	49.7
SA02	34.1	75.4	27.5	66.1	19.4	12.3
SA03	37.5	59.7	17.5	21.9	53.3	63.3
SB01	31.9	48.1	29.6	25.3	7.2	47.4
SB02	38.5	32.2	20.4	18.2	47.0	43.5
SB03	22.3	18.1	18.6	13.7	16.6	24.3
SB04	16.5	22.3	10.5	11.5	36.4	48.4
SB05	17.1	21.8	8.3	15.0	51.5	31.2
SB06	30.8	33.6	11.6	20.5	62.3	39.0

[a] Calculation of RMSE improvement of the simulated sediment concentration is the same as RMSE improvement of current velocity denoted by Eq. (14)
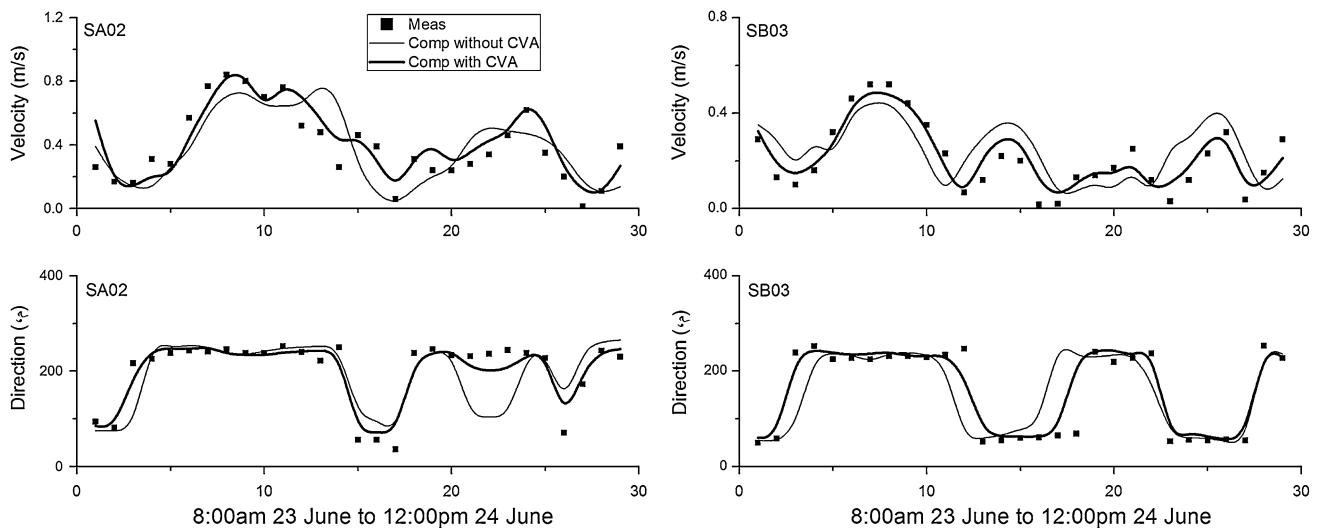
Fig. 4 Depth-averaged velocities for the measurements and computed results using the model with and without CVA at the verification sites SA02 and SB03
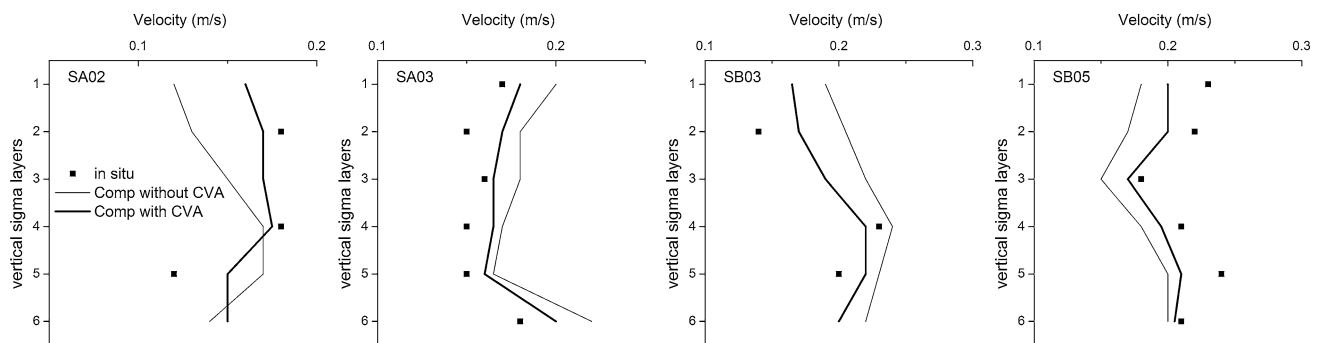
Fig. 5 Comparison of vertical profiles of velocity from measurements and simulated results from the model with and without CVA at the verification sites SA02 and SB03, and assimilation sites SA03 and

SB05 at 10:00 1m on June 23. Note that there were no velocity measurements at some layers at sites SA02 and SB05 because the water depth was very small

distribution of depth-averaged velocities (white arrows) from the model without CVA at maximum ebb and maximum flood tide times, overlaying the assimilated depth-averaged velocity field (red arrows). Such cases also occurred at sites other than the validation sites. Updated velocity field through assimilation is apparently seen in the vicinity of the assimilation sites in the figure. However, because of the sparse distribution of actual measurements, the areas affected by assimilation are limited in extent in relation to the entire model area. Once an updated current velocity pattern has been obtained, a more accurate initial condition is available at the start of the next run period, enabling steady development of increasing accuracy. Therefore, the improvement in the current velocity field is a combination of a 'spatial propagation' effect and a temporal accumulation effect. (Zhang et al. 2007) demonstrated this temporal accumulation effect with an experiment in which current measurements were

assimilated into a flow circulation model. Because this finding is not the focus of this study, further discussion can be found in (Zhang et al. 2007).

3.3 Effect on sediment by CVA

3.3.1 Evaluation by sediment measurements

The ultimate goal of this study, as mentioned in Sect. 1, is the understanding of the effect of current velocity assimilation on sediment transport modeling. The RMSE statistics related to simulated sediment concentration from the model with CVA are given in Table 3. It can be concluded that both near-surface and near-bottom sediment concentrations at all sites are predicted more accurately. The RMSE improvements at all sites are approximately all greater than 10 %. This positive effect also occurs at sites SA02 and SB03, where the measured current velocities
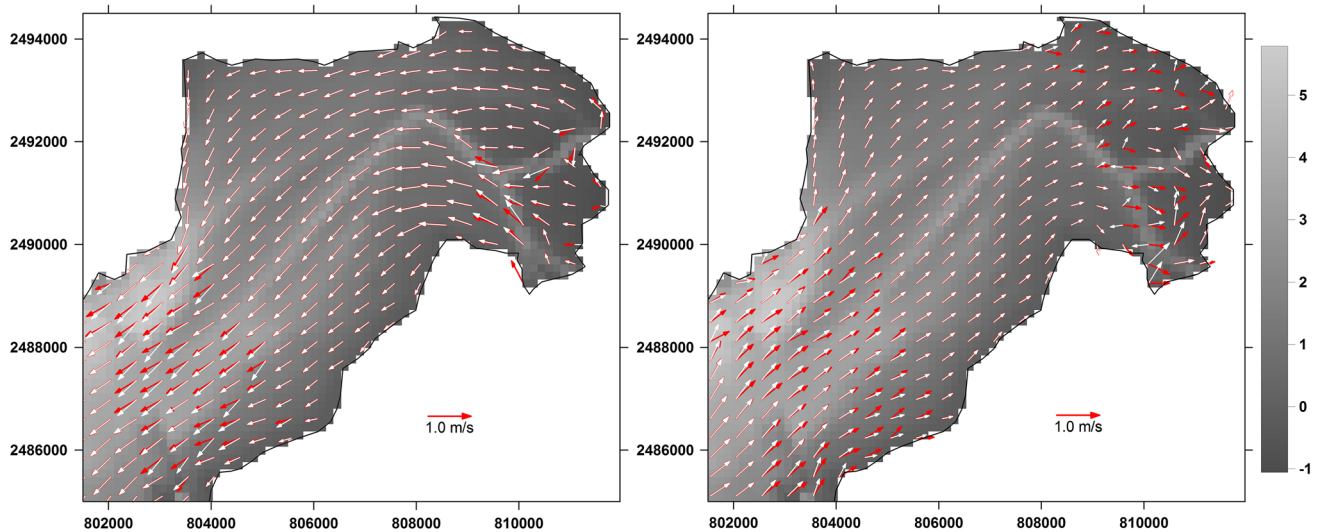
Fig. 6 Spatial distribution of depth-averaged velocity computed from model (*white arrows*) and CVA (*red arrows*) results at ebb time (15:00 pm on June 23) and flood time (09:00 am on June 24). The positions where *white arrow*s accompany *red arrows* indicate obvious current velocity change. Other positions suggest little or no change. The background is the bathymetry of the bay
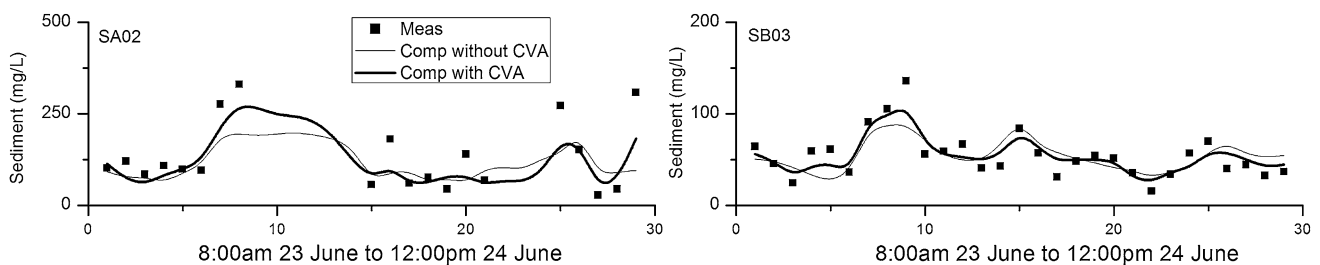
Fig. 7 Sediment concentration comparisons of the measurements and simulated results from the model with and without CVA. *Left* near-bottom sediment concentration at SA02, and *right* depth-averaged sediment concentration at SB03. Note that sometimes the water depth is very small at SA02 and there were no sediment measurements at the near-bottom layer

were not assimilated into the model. The velocity improvement observed at these two sites can be ascribed to the measured velocities assimilated at adjacent sites. However, the improvements in sediment modeling accuracy are greater at most of the velocity assimilation sites than those at the two sites. This is expected because the velocities are periodically updated with exact real velocities in CVA at those assimilation sites.

Figure 7 depicts comparisons of sediment measurements and simulated sediment concentrations from models with and without CVA. This shows that sediment concentrations near the bottom (Fig. 7a) and depth-averaged sediment concentrations (Fig. 7b) computed using models with CVA are in better agreement with the measurements. Comparisons at SB03 show that the model with CVA accurately depicts the variability over time, especially when sediment fluctuations are highly evident. However, for SA02, the simulated sediment from the model with CVA shows no significant improvement in representing variability over

time in the presence of high sediment concentrations; a distinct improvement in simulated current velocity from the model with CVA is found. Many reasons can be possible for these findings, e.g., certain sediment model parameters are not capable of responding to the complex sediment movements in the inner Deep Bay and cannot make the correct response to the fast changing sediment dynamics. Because hydrodynamics are not the only factor controlling sediment motion in water, the positive effect of CVA on the modeling of sediment transport can be limited. The sediment transport modeling requires further investigation.

Figure 8 compares the vertical distributions at Transections A and B, demonstrating that the simulated results from the model with CVA and the measurements are brought into closer agreement in terms of the vertical sediment distribution. To explain this positive effect on the vertical distribution, a comparison of the bottom shear stresses computed from the model with and without CVA

Fig. 8 Vertical sediment distribution at 9:00 am on June 24. TA_1, TA_2, and TA_3 are distributions from the model without CVA, measurements and the model with CVA, respectively, at Transection A. TB_1, TB_2, and TB_3 are distributions from the model without CVA, measurements and the model with CVA, respectively, at Transection B. Note that the water depths in the sites on Transection A (from SA01 to SA03) are 2.3, 2.6, and 4.5 m, respectively. The water depths in the sites on Transection B (from SB01 to SA06) are 7.1, 6.9, 4.3, 5.8, 5.1, and 4.3 m, respectively
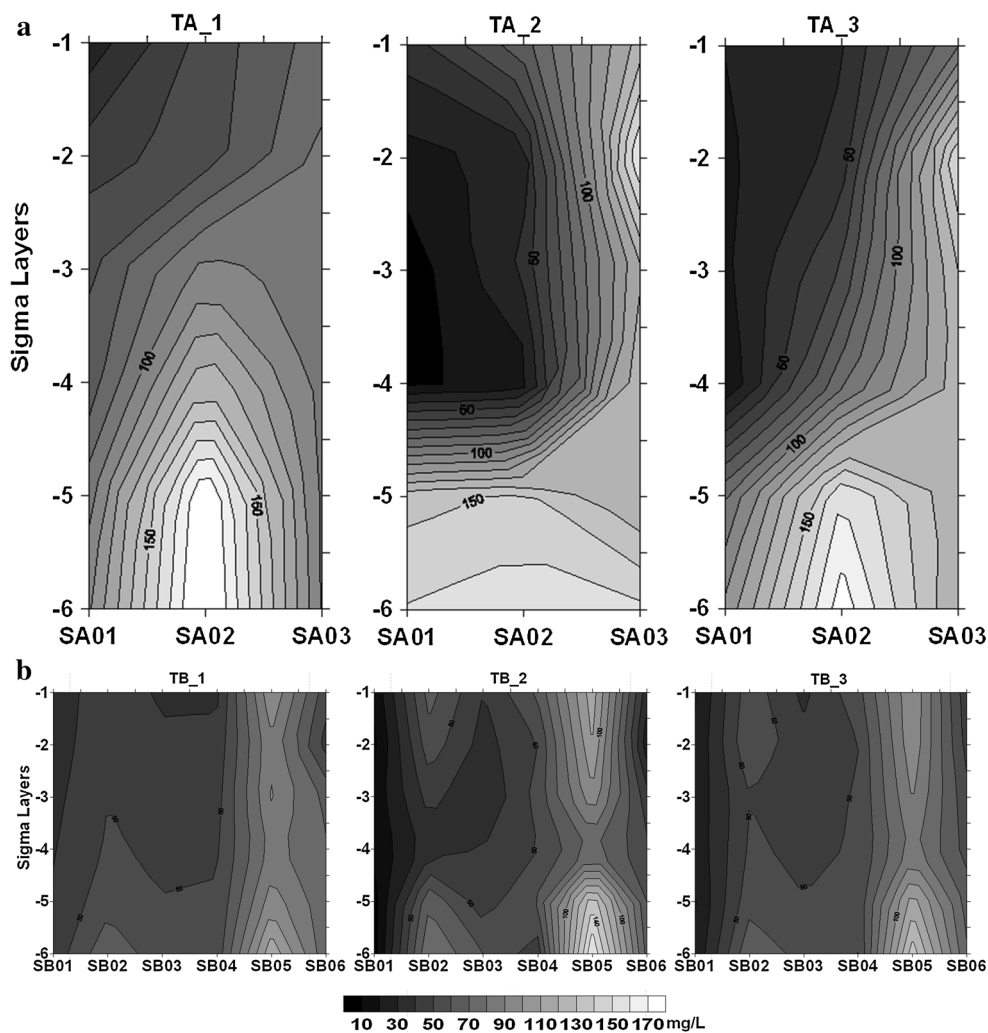
is shown in Fig. 9. Because current velocity assimilation corrects near-bottom boundary velocities, a clear change in the bottom boundary shear stress is seen in Fig. 8. Kurapov et al. (2005) discussed the quantitative improvement in bottom shear stress caused by CVA. However, this study did not associate this improvement with sediment modeling analysis. Figure 8 shows that in Transection A, the surface layer has a low sediment concentration and the bottom layer has a high sediment concentration. Furthermore, it can be seen from the comparison that the model without CVA produced a simulated sediment concentration in the near-bottom layer that is much higher than in the near-surface layer and much higher than the actual measurements taken in the near-bottom layers, especially at site SA02. This inconsistency between the simulated sediment results and the measurements may be the result of excessive bed erosion caused by an excessively large bottom shear stress computed by the hydrodynamic from model without CVA (Fig. 9a). However, the bottom shear stress is corrected, significantly decreased by 50 % at site SA02

after the measured velocity had been assimilated into the model. It is reasonable to believe that the improvement in the vertical sediment distribution when CVA is included (Fig. 8, Transection A) is the result of the shear stress improvement due to CVA. A similar effect is shown in Fig. 8 for Transection B, where the vertical sediment concentration distributions simulated with CVA are closer to the actual measurements than those predicted without CVA. Because the current velocity-based shear stress affects the settling and resuspension processes, achieving a positive sediment modeling effect is expected with a modification to the current velocity in the model with CVA.

3.3.2 Spatial propagation effect of CVA

To study the effect of CVA on the prediction of the spatial sediment distributions, two typical maximum ebb and maximum flood tide periods were selected for analysis. Figure 10 shows selected depth-averaged sediment
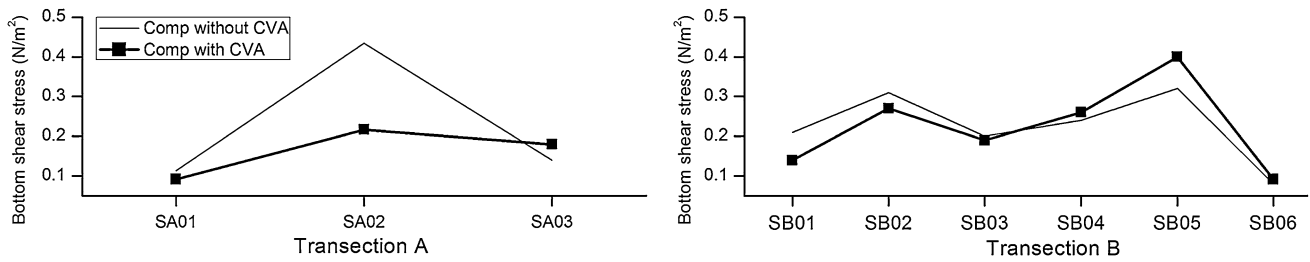
Fig. 9 Magnitude of bottom shear stress computed from the model with and without CVA at the measurement sites along Transection A and Transection B at 9:00 am on June 24
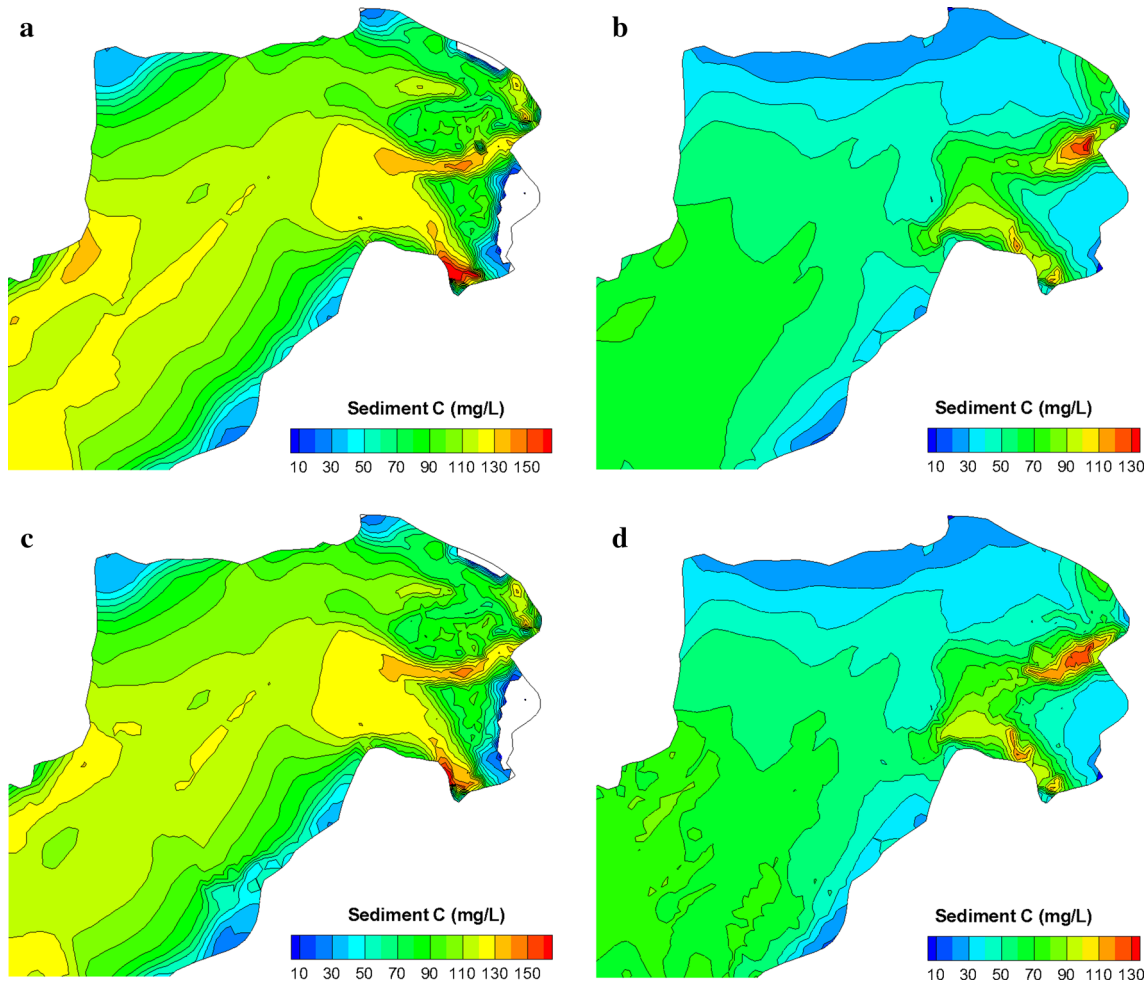
Fig. 10 Spatial distribution of depth-averaged sediment for the results computed using the model with and without CVA at maximum ebb time (**a**, **c**) and maximum flood time (**b**, **d**). **a** and **b** are results from the model without CVA, **c** and **d** are results from the model with CVA

concentrations produced from the model with and without CVA. By comparing the spatial sediment distributions, it can be seen that the simulated sediment concentration changed to some extent after the current velocity data were assimilated into the model. This is not only the result of the direct correction of the hydrodynamic condition that the sediment movement requires but also an indirect result of

the change in the bottom shear stress. However, larger changes in sediment concentrations occurred close to Transections A and B. The effects of CVA on sediment concentrations are limited in extent and only areas close to the measurement sites are affected by CVA. Despite this finding, two distinct distribution changes were observed, the location of the sediment fronts changed near

Transection B and unusually large sediment concentrations near the river mouth decreased. The sediment concentration in the entire area decreased primarily by 5–25 mg/L after including CVA during the maximum ebb tide period. An increase of 5–40 mg/L was found during the maximum flood tide period. A comparison of the two cases indicates that the CVA effect produces greater variation during maximum flood periods in the inner and middle regions of Deep Bay. This result is because the maximum flood period shown in Fig. 10 is at a later stage in the CVA process. Apart from the CVA effect on maximum flood periods, temporal accumulation effects may also affect sediment spatial distribution due to the continuous correction with the latest velocity measurements.

4 Conclusions

A three-dimensional hydrodynamic and sediment transport model for Deep Bay has been established based on a finite volume, unstructured-grid, coastal ocean model. The model has been well calibrated and validated against field measurements and provides a good representation of flow circulations and sediments dynamic in this tide-dominated bay. The model is an important tool that enables further study of long-term sediment transport activities and related environmental issues in Deep Bay.

Because no numerical model provides perfect predictions, additional improvements to the accuracy of the Deep Bay model were achieved using a data assimilation technique. The experiments conducted in this study assimilated the measured three-dimensional current velocity profiles into the model. The widely used optimal interpolation method in oceanic data assimilation was implemented in this study in which both the horizontal and vertical error correlations were considered. The model predictions of flow velocity with measured data assimilated into the model are closer to reality in the vicinities of the measurement stations. The performance of assimilation shows improvements in the root-mean-square errors and average cosine correlations of simulated current velocity by at least 9.1 % and 10.3 %, respectively. In addition, nearby simulated flow velocities were found to more accurately represent the dynamics, indicating the effectiveness of the spatial error covariance model used in the assimilation.

It is believed that current velocity assimilation has a large potential to improve the modeling accuracy of coastal sediment movements because currents dominate sediment dynamics in coastal waters. The results demonstrated that the assimilation also improved the prediction accuracy of three-dimensional sediment transport. The root-mean-square error for the simulated sediment concentration from

the model with CVA was decreased by more than 7 %. A reasonable enhancement in the vertical and spatial distributions of sediment concentrations was demonstrated from the simulation results from the model with CVA. The numerical results also showed a modification of the bottom shear stresses following the correction in the current velocities within the bottom boundary layer due to the assimilation of actual measured current velocities. This modification may be the cause of the improved sediment concentration prediction because of the changes caused to vertical sediment erosion and deposition fluxes.

However, in this study, the velocity assimilation effect on sediment prediction was only observed over limited areas near the measurement locations. This finding may be related to the sparse in situ measurement coving the large model area. Many more current measurements should be collected to enable an in-depth investigation and possibly a better outcome. It is important to note that optimal interpolation is limited to the calculation of time-invariant forecast error covariance. Other data assimilation methods, e.g., the ensemble optimal interpolation and ensemble Kalman filter, may be useful alternatives and increase the scientific perspective as a result of building operational data assimilation systems. Future work could also cover simultaneous assimilation of both current and sediment concentration measurements. Particular focus could be on the assimilation of suspended sediments derived from remote sensing images into three-dimensional hydrodynamic and sediment transport models. As a result, sediment dynamics in coastal and marine waters could be better determined and understood.

References

Barth A, Alvera-Azcárate A, Beckers J-M, Staneva J, Stanev EV, Schulz-Stellenfleth J (2010) Correcting surface winds by assimilating high-frequency radar surface currents in the German Bight. Ocean Dyn 61(5):599–610. doi:10.1007/s10236-010-0369-0

Cancino L, Neves R (1999) Hydrodynamic and sediment suspension modelling in estuarine systems Part I: Description of the numerical models. J Mar Syst 22:105–116. doi:10.1016/S0924-7963(99)00035-4

Chen C, Liu H, Beardsley RC (2003) An unstructured grid, finite-volume, three-dimensional, primitive equations ocean model: application to coastal ocean and estuaries. J Atmos Ocean

Technol 20(1):159–186. doi:10.1175/1520-0426(2003)020<0159:AUGFVT>2.0.CO;2

Chen C, Beardsley RC, Cowles G (2006) An unstructured grid, finite-volume coastal ocean model (FVCOM) System. Oceanography 19(1):78–89

El Serafy GYH, Mynett AE (2008) Improving the operational forecasting system of the stratified flow in Osaka Bay using an ensemble Kalman filter-based steady state Kalman filter. Water Resour Res 44(6):W06416. doi:10.1029/2006wr005412

Galperin B, Kantha L, Hassid S, Rosati A (1988) A quasi-equilibrium turbulent energy model for geophysical flows. J Atmos Sci 45(1):55–62

Grochowski NTL, Collins MB, Boxall SR, Salomon JC, Breton M, Lafite R (1993) Sediment transport pathways in the Eastern English Channel. Oceanol Acta 16(5):531–537

Guillou N, Chapalain G (2010) Numerical simulation of tide-induced transport of heterogeneous sediments in the English Channel. Cont Shelf Res 30(7):806–819. doi:10.1016/j.csr.2010.01.018

Høyer JL, She J (2007) Optimal interpolation of sea surface temperature for the North Sea and Baltic Sea. J Mar Syst 65:176–189. doi:10.1016/j.jmarsys.2005.03.008

Jordi A, Wang D-P (2013) Estimation of transport at open boundaries with an ensemble Kalman filter in a coastal ocean model. Ocean Model 64:56–66. doi:10.1016/j.ocemod.2013.01.002

Krone RB (1962) Flume studies of the transport in estuarine shoaling processes. Hydraulic Engineering Laboratory, University of California, Berkeley

Kurapov AL, Allen JS, Egbert GD, Miller RN, Kosro PM, Levine MD, Boyd T, Barth JA (2005) Assimilation of moored velocity data in a model of coastal wind-driven circulation off Oregon: multivariate capabilities. J Geophys Res 110(C10S08):1–20. doi:10.1029/2004JC002493

Larsen J, Høyer JL, She J (2007) Validation of a hybrid optimal interpolation and Kalman filter scheme for sea surface temperature assimilation. J Mar Syst 65:122–133. doi:10.1016/j.jmarsys.2005.09.013

Lettmann K, Wolff J-O, Liebezeit G, Meier G (2010) Investigation of the spreading and dilution of domestic waste water inputs into a tidal bay using the finite-volume model FVCOM. EGU General Assembly held 2-7 May in Vienna, Austria:p.6139

Lumborg U, Windelin A (2003) Hydrography and cohesive sediment modelling: application to the Rømø Dyb tidal area. J Mar Syst 38:287–303

Margvelashvili N, Andrewartha J, Herzfeld M, Robson BJ, Brando VE (2013) Satellite data assimilation and estimation of a 3D coastal sediment transport model using error-subspace emulators. Environ Model Softw 40:191–201. doi:10.1016/j.envsoft.2012.09.009

Mellor GL, Yamada T (1982) Development of a turbulence closure model for geophysical fluid problems. Rev Geophys 20(4):851–875

Paduan JD (2004) HF radar data assimilation in the Monterey Bay area. J Geophys Res 109(C07S09):1–17. doi:10.1029/2003jc001949

Partheniades E (1965) Erosion and deposition of cohesive soils. J Hydr Div ASCE 91(HY1):105–139

Qian AG (2003) Three-Dimensional Modelling of Hydrodynamics and Tidal Flushing in Deep Bay. Master thesis, The University of Hong Kong, Hong Kong, China

Serafy GY EI, Eleveld MA, Blaas M, Kessel T, Aguilar SG, Woerd HJ (2011) Improving the description of the suspended particulate matter concentrations in the southern North Sea through assimilating remotely sensed data. Ocean Sci J 46(3):179–204. doi:10.1007/s12601-011-0015-x

Smagorinsky J (1963) General circulation experiments with the primitive equations. Mon Weather Rev 91(3):99–164. doi:10.1175/1520-0493(1963)091<0099:gcewtp>2.3.co;2

Warner JC, Sherwood CR, Signell RP, Harris CK, Arango HG (2008) Development of a three-dimensional, regional, coupled wave, current, and sediment-transport model. Comput Geosci 34(10):1284–1306. doi:10.1016/j.cageo.2008.02.012

Wong SH, Li YS (1990) Hydrographic surveys and sedimentation in Deep Bay. Hong Kong. Environ Geol Water Sci 15(2):111–118. doi:10.1007/bf01705098

Wu L, Chen C, Guo P, Shi M, Qi J, Ge J (2011) A FVCOM-based unstructured grid wave, current, sediment transport model, I. Model description and validation. J Ocean Univ China 10(1):1–8. doi:10.1007/s11802-011-1788-3

Xie J, Zhu J (2010) Ensemble optimal interpolation schemes for assimilating Argo profiles into a hybrid coordinate ocean model. Ocean Model 33:283–298. doi:10.1016/j.ocemod.2010.03.002

Zhang Z, Beletsky D, Schwab DJ, Stein ML (2007) Assimilation of current measurements into a circulation model of Lake Michigan. Water Resour Res. doi:10.1029/2006WR005818

Zhang P, Wai O, Chen X, Lu J, Tian L (2014) Improving sediment transport prediction by assimilating satellite images in a Tidal Bay model of Hong Kong. Water 6(3):642–660